RESPONSE OF STIFFNESS AND VISCOSITY ON THE ENERGY RATIOS AT PIEZO-VISCO-THERMO-ELASTIC MEDIUM

Sandeep Kumar and Neelam Kumari
Mathematics, Chaudary Devi Lal, University, Sirsa, INDIA

Vipin Gupta and M.S. Barak[*]
Mathematics, Indira Gandhi University, Meerpur, Rewari, INDIA
E-mail: ms_barak@igu.ac.in

This article presents a mathematical framework that characterizes a transversely isotropic piezo-visco-thermo-elastic medium within the context of the dual-phase lags heat transfer law (PVID) applied to an elastic medium (ES). Specifically, the study investigates the propagation of plane waves within the elastic medium and their interaction with the imperfect interface of the ES/PVID media. This interaction results in two waves reflecting back into the elastic medium and four waves propagating through the piezo-visco-thermo-elastic medium. The research explores the distribution of energy between the reflected and transmitted waves by analyzing amplitude ratios at the boundary interfaces, considering factors such as phase delays, viscosity effects, and wave frequency. The study illustrates the influence of boundary stiffness and viscosity parameters on these energy ratios through graphical re*P*resentations. The study's findings are consistent with the principles of the energy balance law, and the research also delves into specific cases of interest. Overall, this investigation provides insights into wave behavior within complex media and offers potential applications across various fields.

Key words: dual-phase lag; energy ratios; imperfect interfaces; piezo-thermoelastic; viscosity.

1. Introduction

In recent years, researchers have shown considerable interest in investigating various models of an elastic solid under distinct physical fields, such as viscous, thermal, piezoelectric, and others. Among these materials, the piezoelectric material is from the core of modern studies and investigation.

Mindlin [1] is recognized as the trailblazer in establishing the governing equation for thermal piezo-elastic materials. Building upon Mindlin's work, Nowacki [2, 3] further elaborated on the foundational principles governing thermal piezo-elastic substances. Utilizing Mindlin's theory of piezo-thermoelasticity, Chandrasekharaiah [4] investigated the propagation of thermal disturbances at finite speeds. The study of how plane waves interact with various materials, particularly in terms of their reflection and transmission properties, has captured substantial attention from researchers across time. This subject has undergone extensive examination, evident from the comprehensive range of references cited in the literature[5-11]. Notably, Gupta and colleagues [12-17] made a significant contribution to this domain through their remarkable research on wave propagation at the interface of a piezo-thermo-elastic material. In their work, they harnessed advanced modeling techniques, specifically the dual-phase lags (DPL) and three-phase lags (TPL) memory-dependent derivative (MDD) models. These choices were driven by the models' capability to accurately capture the intricate behavior of the material under scrutiny. Moreover, Gupta's investigation incorporated diverse temperature theories to enhance the comprehensiveness of their analysis.

Viscous materials like amorphous, polymers, semi-crystalline, and bio-polymers play a predominant role in many branches of civil, geotechnical, and biomechanical engineering. An extensively recognized macroscopic mechanical framework utilized to illustrate the viscoelastic properties of materials is described

---

[*] To whom correspondence should be addressed

in [18]. This model elucidates the manner in which an elastic material reacts to stress under conditions where deformation is time-dependent yet reversible. Many investigators worked on the different problems of viscoelastic and thermo-viscoelastic such as [19-26]. Lotfy and his team conduct extensive research on problems related to piezothermoelastic media with photothermal effects, focusing on the hyperbolic two-temperature model [26-31].

This article aims to investigate the energy distribution between reflected and transmitted waves at the interface of transversely isotropic piezo-visco-thermoelastic and elastic half-spaces, considering their imperfections. The analysis is based on the dual-phase lags heat transfer law and focuses on the heat conduction process for incident *P* or *SV* waves. This study examines the influence of viscosity and boundary contacts on various energy ratios, and presents the findings through visual representations.

2. Basic governing equations

The fundamental equations describing an anisotropic piezo-visco-thermoelastic material within the framework of the DPL heat model, in the absence of both heat sources and body forces, are provided by Voigt [18], Gupta *et al.* [14], and Tzou [32] as follows

$$\sigma_{ij} = \bar{c}_{ijro}\, e_{ro} - \eta_{ijr}\, E_r - \beta_{ij}\, T \ , \tag{2.1}$$

$$\sigma_{ij,j} = \rho\, \ddot{u}_i \ , \tag{2.2}$$

$$E_i = -\varphi_{,i} \ , \tag{2.3}$$

$$D_i = \tau_i\, T + \eta_{ijr}\, e_{jr} + \varepsilon_{ij} E_j \ , \tag{2.4}$$

$$D_{i,i} = 0 \ , \tag{2.5}$$

$$\left(1 + \tau_T \frac{\partial}{\partial t}\right) K_{ij} T_{,ij} = \left(1 + \tau_q \frac{\partial}{\partial t} + \frac{\tau_q^2}{2}\frac{\partial^2}{\partial t^2}\right)\left(T_0\left(\beta_{ij}\dot{u}_{i,j} - \tau_i\dot{\varphi}_{,i}\right) + \rho C_E \dot{T}\right) , \tag{2.6}$$

where,
$$\bar{c}_{ijro} = c_{ijro} + c_{ijro}^v\,\frac{\partial}{\partial t}\,, \quad \beta_{ij} = \bar{c}_{ijro}\alpha_{ro}^* \ . \tag{2.7}$$

Achenbach [33] provides the following field equations for an elastic solid without body forces:

$$\sigma_{ij}^e = \mu^e\,(u_{i,j}^e + u_{j,i}^e) + \lambda^e\, u_{r,r}^e\, \delta_{ij} \ , \tag{2.8}$$

$$\sigma_{ij,j}^e = \rho^e\, \ddot{u}_i^e \ , \qquad (i,j,o,r = 1,2,3) \ . \tag{2.9}$$

2.1. Limiting cases

- If $\tau_q = \tau_T = 0$ in Eq.(2.6), then the current model transforms into Biot [34] model.
- If $\tau_q > 0$, $\tau_q^2 = \tau_T = 0$ in Eq.(2.6), then converts into Lord and Shulman [35] model.

3. Problem formulation

A half-space with transversely isotropic piezo-visco-thermoelastic properties with dual phase lag, referred to as (PVID) ($x_3 > 0$), is considered in conjunction with an elastic half-space *ES* ($x_3 < 0$). The interface between these two materials is imperfect and is depicted in Fig.1. The plane wave propagates within the $x_1x_3 -$ plane, and in the context of this two-dimensional problem, we take $\vec{u}$ and $\vec{u}^e$ as

$$\vec{u} = (u_1, 0, u_3), \tag{3.1}$$

$$\vec{u}^e = (u_1^e, 0, u_3^e). \tag{3.2}$$

The constitutive equations governing the behavior of the PVID in the $x_1x_3 -$ plane are given as

$$\sigma_{33} = \overline{c}_{13}\, u_{1,1} + \overline{c}_{33}\, u_{3,3} + \eta_{33}\, \varphi_{,3} - \beta_{33}\, T\,, \tag{3.3}$$

$$\sigma_{13} = \overline{c}_{44}\left(u_{1,3} + u_{3,1}\right) + \eta_{15}\, \varphi_{,1}\,, \tag{3.4}$$

$$\sigma_{11} = \overline{c}_{11}\, u_{1,1} + \overline{c}_{13}\, u_{3,3} + \eta_{31}\, \varphi_{,3} - \beta_{11}\, T\,, \tag{3.5}$$

$$D_1 = \eta_{15}\left(u_{1,3} + u_{3,1}\right) - \varepsilon_{11}\varphi_{,1}\,, \tag{3.6}$$

$$D_3 = \eta_{31}\, u_{1,1} + \eta_{33}\, u_{3,3} - \varepsilon_{33}\varphi_{,3} + \tau_3\, T\,, \tag{3.7}$$

where $\beta_{11} = \left(c_{11} + c_{12}\right)\alpha_{11} + c_{13}\alpha_{33}$, $\beta_{33} = 2c_{13}\alpha_{11} + c_{33}\alpha_{33}$.

The constitutive equations for the *ES* in the $x_1x_3 -$ plane are given below

$$\sigma_{33}^e = \lambda^e\left(u_1^e{}_{,1} + u_{3,3}^e\right) + 2\mu^e u_{3,3}^e\,, \tag{3.8}$$

$$\sigma_{13}^e = \mu^e\left(u_1^e{}_{,3} + u_{3,1}^e\right), \tag{3.9}$$

$$\sigma_{11}^e = \lambda^e\left(u_1^e{}_{,1} + u_{3,3}^e\right) + 2\mu^e u_{1,1}^e\,. \tag{3.10}$$

Equations (2.1)-(2.7) and (3.1)-(3.7) produce the governing equations for the two-dimensional PVID medium as

$$\overline{c}_{11}u_{1,11} + \left(\overline{c}_{13} + \overline{c}_{44}\right)u_{3,13} + \overline{c}_{44}u_{1,33} - \beta_1 T_{,1} + \left(\eta_{31} + \eta_{15}\right)\varphi_{,13} - \rho\ddot{u}_1 = 0\,, \tag{3.11}$$

$$\left(\overline{c}_{13} + \overline{c}_{44}\right)u_{1,13} + \overline{c}_{33}u_{3,33} + \overline{c}_{44}u_{3,11} - \beta_3 T_{,3} + \eta_{15}\varphi_{,11} + \eta_{33}\varphi_{,33} - \rho\ddot{u}_3 = 0\,, \tag{3.12}$$

$$\left(1 + \tau_T\frac{\partial}{\partial t}\right)\left(K_1 T_{,11} + K_3 T_{,33}\right) = \left(1 + \tau_q\frac{\partial}{\partial t} + \frac{\tau_q^2}{2}\frac{\partial^2}{\partial t^2}\right)\left(T_0\left(\beta_1\dot{u}_{1,1} + \beta_3\dot{u}_{3,3} - \tau_3\dot{\varphi}_{,3}\right) + \rho C_E\dot{T}\right), \tag{3.13}$$

$$\left(\eta_{15}+\eta_{31}\right)u_{1,13}+\eta_{15}u_{3,11}+\eta_{33}u_{3,33}+\tau_3 T_{,3}-\varepsilon_{11}\varphi_{,11}-\varepsilon_{33}\varphi_{,33}=0\,, \tag{3.14}$$

where, $\beta_{ij}=\beta_i\delta_{ij}$, $K_{ij}=K_i\delta_{ij}$, and here i is not included in the summation.

The non-dimensional quantities can be used as

$$\left(\sigma_{ij}{}',\sigma_{ij}^e{}'\right)=\frac{1}{\beta_1 T_0}\left(\sigma_{ij},\sigma_{ij}^e\right),\quad\left(x_1{}',x_3{}',\right)=\frac{\omega_1}{c_1}(x_1,x_3),\quad\left(u_1{}',u_3{}'\right)=\frac{\omega_1}{c_1}\left(u_1,u_3\right),$$

$$t'=\omega_1 t,\quad\left(u_1^e{}',u_3^e{}'\right)=\frac{\omega_1}{c_1}\left(u_1^e,u_3^e\right),\quad\varphi'=\frac{\omega_1\eta_{31}}{c_1\beta_1 T_0}\varphi,$$

$$\left(\tau_T{}',\tau_q{}'\right)=\omega_1\left(\tau_T,\tau_q\right),\ T'=\frac{\beta_1}{\rho c_1^2}T,\ D_3{}'=\frac{c_{11}D_3}{\eta_{33}\beta_1 T_0}, \tag{3.15}$$

where $\qquad c_1=\sqrt{\dfrac{c_{11}}{\rho}}\ ,\ \ \omega_1=\dfrac{\rho C_E c_1^2}{K_1}.$

By utilizing Eq.(3.15) and removing the primes $(')$, we can express Eqs. (3.11)-(3.14), and (2.8), (2.9) in the following form

$$\left(\frac{\partial^2}{\partial x_1^2}+a_{11}\frac{\partial^2}{\partial x_3^2}-\frac{\partial^2}{\partial t^2}\right)u_1+a_{12}\frac{\partial^2 u_3}{\partial x_1\partial x_3}+a_{13}\frac{\partial^2\varphi}{\partial x_1\partial x_3}-\frac{\partial T}{\partial x_1}=0\,, \tag{3.16}$$

$$\frac{\partial^2 u_1}{\partial x_1\partial x_3}+\left(a_{21}\frac{\partial^2}{\partial x_1^2}+a_{22}\frac{\partial^2}{\partial x_3^2}-a_{23}\frac{\partial^2}{\partial t^2}\right)u_3+\left(a_{24}\frac{\partial^2}{\partial x_1^2}+a_{25}\frac{\partial^2}{\partial x_3^2}\right)\varphi-a_{26}\frac{\partial T}{\partial x_3}=0, \tag{3.17}$$

$$\left(1+\tau_T\frac{\partial}{\partial t}\right)\left(a_{31}\frac{\partial^2}{\partial x_1^2}+a_{32}\frac{\partial^2}{\partial x_3^2}\right)T+$$
$$-\left(1+\tau_q\frac{\partial}{\partial t}+\frac{\tau_q^2}{2}\frac{\partial^2}{\partial t^2}\right)\left(\frac{\partial^2\dot{u}_1}{\partial x_1}+a_{33}\frac{\partial^2\dot{u}_3}{\partial x_3}-a_{34}\frac{\partial\dot{\varphi}}{\partial x_3}+a_{35}\dot{T}\right)=0, \tag{3.18}$$

$$\frac{\partial^2 u_1}{\partial x_1\partial x_3}+\left(a_{41}\frac{\partial^2}{\partial x_1^2}+a_{42}\frac{\partial^2}{\partial x_3^2}\right)u_3-\left(a_{43}\frac{\partial^2}{\partial x_1^2}+a_{44}\frac{\partial^2}{\partial x_3^2}\right)\varphi+a_{45}\frac{\partial T}{\partial x_3}=0\,, \tag{3.19}$$

$$\left(\frac{\alpha^{e^2}-\beta^{e^2}}{c_1^2}\right)\left(\frac{\partial^2 u_1^e}{\partial x_1^2}+\frac{\partial^2 u_3^e}{\partial x_3\,\partial x_1}\right)+\frac{\beta^{e^2}}{c_1^2}\left(\frac{\partial^2 u_1^e}{\partial x_1^2}+\frac{\partial^2 u_1^e}{\partial x_3^2}\right)=\frac{\partial^2 u_1^e}{\partial t^2}\,, \tag{3.20}$$

$$\left(\frac{\alpha^{e2}-\beta^{e2}}{c_1^2}\right)\left(\frac{\partial^2 u_1^e}{\partial x_3 \partial x_1}+\frac{\partial^2 u_3^e}{\partial x_3^2}\right)+\frac{\beta^{e2}}{c_1^2}\left(\frac{\partial^2 u_3^e}{\partial x_1^2}+\frac{\partial^2 u_3^e}{\partial x_3^2}\right)=\frac{\partial^2 u_3^e}{\partial t^2}, \tag{3.21}$$

where

$$a_{11}=\frac{\overline{c}_{44}}{\overline{c}_{11}}, \quad a_{12}=\frac{\overline{c}_{13}+\overline{c}_{44}}{\overline{c}_{11}}, \quad a_{13}=\frac{\eta_{31}+\eta_{15}}{c_{11}\eta_{31}}\beta_1 T_0, \quad a_{21}=\frac{\overline{c}_{44}}{\overline{c}_{44}+\overline{c}_{13}}, \quad a_{22}=\frac{\overline{c}_{33}}{\overline{c}_{44}+\overline{c}_{13}},$$

$$a_{23}=\frac{\overline{c}_{11}}{\overline{c}_{44}+\overline{c}_{13}}, \quad a_{24}=\frac{\eta_{15}\beta_1 T_0}{\eta_{31}(\overline{c}_{44}+\overline{c}_{13})}, \quad a_{25}=\frac{\eta_{33}\beta_1 T_0}{\eta_{31}(\overline{c}_{44}+\overline{c}_{13})}, \quad a_{26}=\frac{\overline{c}_{11}\beta_3}{(\overline{c}_{44}+\overline{c}_{13})\beta_1},$$

$$a_{31}=\frac{K_1\omega_1\rho}{T_0\beta_1^2}, \quad a_{32}=\frac{K_3\omega_1\rho}{T_0\beta_1^2}, \quad a_{33}=\frac{\beta_3}{\beta_1}, \quad a_{34}=\frac{\tau_3 T_0}{\eta_{31}}, \quad a_{35}=\frac{c_{11}\rho C_E}{T_0\beta_1^2},$$

$$a_{41}=\frac{\eta_{15}}{(\eta_{15}+\eta_{31})}, \quad a_{42}=\frac{\eta_{33}}{(\eta_{15}+\eta_{31})}, \quad a_{43}=\frac{\varepsilon_{11}\beta_1 T_0}{\eta_{31}(\eta_{15}+\eta_{31})}, \quad a_{44}=\frac{\varepsilon_{33}\beta_1 T_0}{\eta_{31}(\eta_{15}+\eta_{31})},$$

$$a_{45}=\frac{c_{11}\tau_3}{\beta_1(\eta_{15}+\eta_{31})}, \quad \beta^e=\sqrt{\frac{\mu^e}{\rho^e}}, \quad \alpha^e=\sqrt{\frac{\lambda^e+2\mu^e}{\rho^e}}.$$

Using the Helmholtz principle, the displacement components in *ES* may be stated as

$$u_1^e=\frac{\partial\varphi^e}{\partial x_1}-\frac{\partial\psi^e}{\partial x_3}, \quad u_3^e=\frac{\partial\varphi^e}{\partial x_3}+\frac{\partial\psi^e}{\partial x_1}, \tag{3.22}$$

where the potential functions φ^e and ψ^e meet the subsequent wave equations

$$\nabla^2\psi^e=\frac{\ddot{\psi}^e}{\beta^{*2}}, \quad \nabla^2\varphi^e=\frac{\ddot{\varphi}^e}{\alpha^{*2}} \quad \text{and} \quad \alpha^*=\frac{\alpha^e}{c_1}, \ \beta^*=\frac{\beta^e}{c_1}. \tag{3.23}$$

4. Investigation of wave propagation

Consider the PVID medium to have a plane wave form solution and express it as

$$(u_1, u_3, \varphi, T)(x_1, x_3, t)=(H, M, N, U)\exp\left[\iota\omega\left(-\frac{x_1}{c}-q x_3+t\right)\right], \tag{4.1}$$

where H, M, N, U indicates the amplitude coefficient.

The homogeneity of a system can be obtained by incorporating Eq.(4.1) into a set of Eqs. (3.16)-(3.19).

$$\Omega R = 0, \tag{4.2}$$

$$\Omega = \begin{bmatrix} l_{11}+q^2 l_{12} & ql_{13} & ql_{14} & -l_{15} \\ qc & l_{21}+q^2 l_{22} & a_{24}+q^2 l_{23} & -ql_{24} \\ c & ql_{31} & -ql_{32} & l_{33}+q^2 l_{34} \\ cq & a_{41}+q^2 l_{41} & -a_{43}-q^2 l_{42} & ql_{43} \end{bmatrix}, \quad R = \begin{bmatrix} H \\ M \\ N \\ U \end{bmatrix}, \tag{4.3}$$

where

$$l_{11}=c-c^3, \quad l_{12}=a_{11}c^3, \quad l_{13}=a_{12}c^2, \quad l_{14}=a_{13}c^2, \quad l_{15}=\frac{\iota c^2}{\omega},$$

$$l_{21}=a_{21}-a_{23}c^2, \quad l_{22}=a_{22}c^2, \quad l_{23}=a_{25}c^2, \quad l_{24}=\frac{\iota a_{26} c^2}{\omega},$$

$$l_{31}=a_{35}c^2, \quad l_{32}=a_{36}c^2, \quad l_{33}=\frac{(1+\tau_T \iota\omega)a_{33}}{1+\tau_q \iota\omega - \tau_q^2 \omega^2/2}-\frac{a_{37}c^2}{\iota\omega}, \quad l_{34}=\frac{(1+\tau_T \iota\omega)a_{34}c^2}{1+\tau_q \iota\omega - \tau_q^2 \omega^2/2},$$

$$l_{41}=c^2 a_{42}, \quad l_{42}=c^2 a_{44}, \quad l_{43}=\frac{\iota c^2 a_{45}}{\omega}.$$

The existence of a non-trivial solution for a system of equations represented by Eq. (4.2) results in the formulation of a characteristic equation.

$$G_{11}q^8 + G_{12}q^6 + G_{13}q^4 + G_{14}q^2 + G_{15} = 0. \tag{4.4}$$

The MATLAB software is utilized to solve Eq. (4.4), and the roots are arranged in decreasing order of magnitude. For our convenience, we have labeled them as follows: q_i $(i=1-4)$ denotes the roots that include positive imaginary parts and q_i $(i=5-8)$ depicts the roots that contain negative imaginary parts. The propagation of waves in the electric potential mode (eP) is associated with the eigenvalue q_4. The quasi-propagating modes q_i $(i=1-3)$, are quasi-P (qP), quasi-T (qT), and quasi-S (qS), respectively. The value of the coefficients G_{1i} $(i=1-5)$ may be found in Appendix A.

Corresponding to each eigenvalue q_i $(i=1-8)$, the H_i, M_i, N_i, and U_i eigenvectors can be expressed as

$$W_i = \frac{cf(\Omega_{42})_{q_i}}{cf(\Omega_{41})_{q_i}}, \quad \Phi_i = \frac{cf(\Omega_{43})_{q_i}}{cf(\Omega_{41})_{q_i}}, \quad \Theta_i = \frac{cf(\Omega_{44})_{q_i}}{cf(\Omega_{41})_{q_i}}, \tag{4.5}$$

where

$$W_i = \frac{M_i}{H_i}, \quad \Phi_i = \frac{N_i}{H_i}, \quad \Theta_i = \frac{U_i}{H_i}, \tag{4.6}$$

and corresponding to the eigenvalue q_i, $cf(\Omega_{ij})_{q_i}$ denote the cofactor Ω_{ij}.

The wave equations solution in the *ES* medium may be written as

$$\varphi^e = A_0^e \exp\left[\iota\omega\left(\frac{-x_1\sin\theta_0 - x_3\cos\theta_0}{\alpha^*} + t\right)\right] + A_1^e \exp\left[\iota\omega\left(\frac{-x_1\sin\theta_0 + x_3\cos\theta_0}{\alpha^*} + t\right)\right], \quad (4.7)$$

$$\psi^e = B_0^e \exp\left[\iota\omega\left(\frac{-x_1\sin\theta_0 - x_3\cos\theta_0}{\beta^*} + t\right)\right] + B_1^e \exp\left[\iota\omega\left(\frac{-x_1\sin\theta_0 + x_3\cos\theta_0}{\beta^*} + t\right)\right]. \quad (4.8)$$

5. Refraction and reflection coefficients

It is assumed that when a plane wave, either *P* or *SV*, propagates through the *ES* medium and impinges upon the interface at an angle θ_0 relative to the x_3 – axis, it has the potential to generate two reflected waves within the *ES* medium and four transmitted waves within the PVID media.

The non-dimensional displacement and stress components, electric potential, thermal temperature, and electric displacement in a PVID medium can be expressed using Eqs. (3.3), (3.4), (3.7), (3.15), (4.1), and (4.6) as

$$(u_1, u_3, \varphi, T) = \sum_{i=1}^{4}(1, W_i, \Phi_i, \Theta_i)H_i \exp\left[\iota\omega\left(-\frac{x_1}{c} - q_i x_3 + t\right)\right], \quad (5.1)$$

$$(\sigma_{33}, \sigma_{31}, D_3) = \iota\omega\sum_{i=1}^{4}(\Delta_{1i}, \Delta_{2i}, \Delta_{6i})H_i \exp\left[\iota\omega\left(-\frac{x_1}{c} - q x_3 + t\right)\right], \quad (5.2)$$

where

$$\Delta_{1i} = -\frac{c_{13}}{\beta_1 T_0 c} - \left(\frac{c_{33}W_i}{\beta_1 T_0} + \frac{\eta_{33}}{\eta_{31}}\Phi_i\right)q_i - \frac{c_{11}\beta_3}{\iota\omega\beta_1^2 T_0}\Theta_i, \qquad \Delta_{2i} = -\frac{c_{44}W_i}{\beta_1 T_0 c} - \frac{c_{44}q_i}{\beta_1 T_0} - \frac{\eta_{15}\Phi_i}{c\eta_{31}},$$

$$\Delta_{6i} = \left(-\eta_{33}W_i + \frac{\varepsilon_{33}\beta_1 T_0}{\eta_{31}}\Phi_i\right)\frac{c_{11}q_i}{\eta_{33}\beta_1 T_0} - \frac{c_{11}\eta_{31}}{\eta_{33}\beta_1 T_0 c} + \frac{c_{11}^2\tau_3}{\eta_{33}\beta_1^2 T_0\iota\omega}\Theta_i, \qquad i = 1 - 4.$$
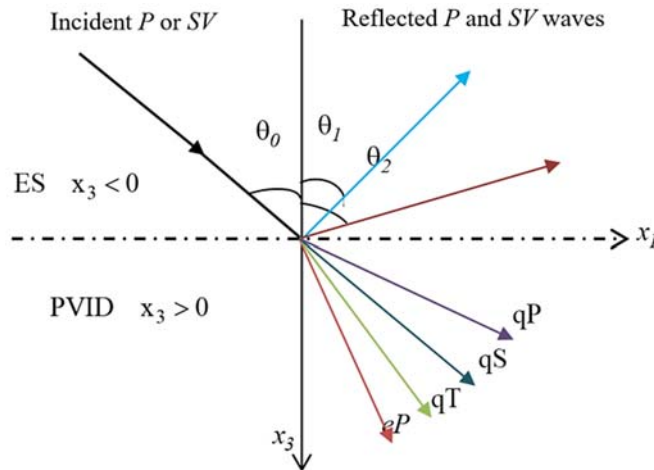
Fig.1. Reflection and refraction of plane waves in *ES* and PVID.

5.1. Boundary conditions

The following boundary conditions are assumed to solve this problem, *i.e.,* equally normal and tangential stress distribution, discontinuity for mechanical displacement due to imperfect contact of *ES* and PVID media, thermal insulated, and vanishing of electric displacement at an interface, $x_3 = 0$:

$$\sigma_{33} = \sigma_{33}^e, \quad \sigma_{31} = \sigma_{31}^e, \quad \sigma_{33} = K_n\left(u_3 - u_3^e\right), \quad \sigma_{13} = K_t\left(u_1 - u_1^e\right), \quad \frac{\partial T}{\partial x_3} = 0, \quad D_3 = 0, \quad (5.3)$$

where K_t, K_n, indicate the transverse and normal force stiffness coefficients of a unit layer thickness, respectively.

Inserting the values of φ^e, ψ^e, and $\left(u_1, u_3, \varphi, T\right)$ from (4.7), (4.8), (5.1), (5.2) in the boundary conditions (5.3) and with (3.8), (3.9), (3.15), (3.22) yield the non-homogenous system of equations. which may be written as

$$\Delta X = Q, \tag{5.4}$$

where

$$\Delta = \begin{bmatrix} \Delta_{11} & \Delta_{12} & \Delta_{13} & \Delta_{14} & \Delta_{15} & \Delta_{16} \\ \Delta_{21} & \Delta_{22} & \Delta_{23} & \Delta_{24} & \Delta_{25} & \Delta_{26} \\ \Delta_{31} & \Delta_{32} & \Delta_{33} & \Delta_{34} & \Delta_{35} & \Delta_{36} \\ \Delta_{41} & \Delta_{42} & \Delta_{43} & \Delta_{44} & \Delta_{45} & \Delta_{46} \\ \Delta_{51} & \Delta_{52} & \Delta_{53} & \Delta_{54} & 0 & 0 \\ \Delta_{61} & \Delta_{62} & \Delta_{63} & \Delta_{64} & 0 & 0 \end{bmatrix}, \quad X = \begin{bmatrix} X_1 \\ X_2 \\ X_3 \\ X_4 \\ X_5 \\ X_6 \end{bmatrix}, \quad Q = \begin{bmatrix} Q_1 \\ Q_2 \\ Q_3 \\ Q_4 \\ 0 \\ 0 \end{bmatrix}.$$

$$\Delta_{3i} = \iota\omega\left(\frac{\Delta_{2i}}{k_t} + \frac{1}{\iota\omega}\right), \quad \Delta_{4i} = \iota\omega\left(\frac{\Delta_{1i}}{k_n} + \frac{W_i}{\iota\omega}\right), \quad D_{5i} = \Theta_i q_i, \quad i = 1-4.$$

(i) For incident *P* wave

$$\Delta_{15} = -\frac{\iota\omega\rho^e c_1^2}{\beta_1 T_0}\left[1 - \frac{2\beta^{e2}\sin^2\theta_0}{\alpha^{e2}}\right], \quad \Delta_{16} = \frac{\iota\omega\rho^e c_1^2 \sin 2\theta_2}{\beta_1 T_0},$$

$$\Delta_{25} = \frac{\iota\omega\beta^{e2}\rho^e c_1^2 \sin 2\theta_0}{\beta_1 T_0 \alpha^{e2}}, \quad \Delta_{26} = \frac{\iota\omega\rho^e c_1^2 \cos 2\theta_2}{\beta_1 T_0},$$

$$\Delta_{35} = \frac{\iota\omega\sin\theta_0}{\alpha^*}, \quad \Delta_{36} = \frac{\iota\omega\cos\theta_2}{\beta^*}, \quad \Delta_{45} = -\frac{\iota\omega\cos\theta_0}{\alpha^*}, \quad \Delta_{46} = \frac{\iota\omega\sin\theta_2}{\beta^*},$$

$$X_i = \frac{H_i}{A_0^e}, (i = 1-4), \quad X_5^e = \frac{A_1^e}{A_0^e}, \quad X_6^e = \frac{B_1^e}{A_0^e},$$

$$N_1 = -\Delta_{15}, \quad N_2 = \Delta_{25}, \quad N_3 = -\Delta_{35}, \quad N_4 = \Delta_{45}.$$

(ii) For incident *SV* wave

$$\Delta_{15} = -\frac{\iota\omega\rho^e c_1^2}{\beta_1 T_0}\left[1 - \frac{2\beta^{e2}\sin^2\theta_1}{\alpha^{e2}}\right], \quad \Delta_{16} = \frac{\iota\omega\rho^e c_1^2 \sin 2\theta_0}{\beta_1 T_0},$$

$$\Delta_{25} = \frac{\iota\omega\beta^{e2}\rho^e c_1^2 \sin 2\theta_1}{\beta_1 T_0 \alpha^{e2}}, \quad \Delta_{26} = \frac{\iota\omega\rho^e c_1^2 \cos 2\theta_0}{\beta_1 T_0},$$

$$\Delta_{35} = \frac{\iota\omega\sin\theta_1}{\alpha^*}, \quad \Delta_{36} = \frac{\iota\omega\cos\theta_0}{\beta^*}, \quad \Delta_{45} = -\frac{\iota\omega\cos\theta_1}{\alpha^*}, \quad \Delta_{46} = \frac{\iota\omega\sin\theta_0}{\beta^*},$$

$$Q_1 = \Delta_{16}, \quad Q_2 = -\Delta_{26}, \quad Q_3 = \Delta_{36}, \quad Q_4 = -\Delta_{46}.$$

6. Energy ratios

Following [14] determine the distribution of energy between different reflected waves within *ES* medium and transmitted waves within PVID medium, occurring at the imperfect interface across a unit area of the surface element is determined as

$$P = -\mathrm{Re}\left(\sigma_{13}\bar{u}_1 + \sigma_{33}\bar{u}_3 - \varphi\bar{D}_3 + K_3\bar{T},_3\frac{T}{T_0}\right), \tag{6.1}$$

and for the *ES* material

$$P^e = -\mathrm{Re}\left(\sigma_{31}^e\bar{u}_1^e + \sigma_{33}^e\bar{u}_3^e\right). \tag{6.2}$$

The average energy fluxes for

(i)   incident waves (*P* or *SV*)

$$\left\langle P_{IP}^e\right\rangle = \frac{1}{2\alpha^*}\omega^4\rho^e c_1^2\,\mathrm{Re}(\cos\theta_0)\left|A_0^e\right|^2, \quad \left\langle P_{IS}^e\right\rangle = \frac{1}{2\beta^*}\omega^4\rho^e c_1^2\,\mathrm{Re}(\cos\theta_0)\left|B_0^e\right|^2, \tag{6.3}$$

(ii) reflected waves (*P* and *SV*)

$$\left\langle P_{RP}^e\right\rangle = -\frac{1}{2\alpha^*}\omega^4\rho^e c_1^2\,\mathrm{Re}(\cos\theta_1)\left|A_1^e\right|^2, \quad \left\langle P_{RS}^e\right\rangle = -\frac{1}{2\beta^*}\omega^4\rho^e c_1^2\,\mathrm{Re}(\cos\theta_2)\left|B_1^e\right|^2, \tag{6.4}$$

(iii) transmitted waves (*qP*, qS, *qT* and *eP*)

$$\left\langle P_s\right\rangle = \frac{1}{2}\omega^2\,\mathrm{Re}\left(\Delta_{2s} + \Delta_{1s}\bar{W}_s + \bar{\Delta}_{6s}\Phi_s + \frac{\iota}{\omega}\frac{K_3}{T_0}\bar{\Delta}_{5s}\Theta_s\right)\left|H_s\right|^2, \quad (s = 1,2,3,4). \tag{6.5}$$

(a) For incident P wave

The energy ratios of the reflected waves (P and SV):

$$E_{RP} = \frac{\langle P_{RP}^e \rangle}{\langle P_{IP}^e \rangle}, \quad E_{RS} = \frac{\langle P_{RS}^e \rangle}{\langle P_{IP}^e \rangle},$$

(6.6)

and the transmitted waves (qP, qSV, qT, and eP):

$$ES_s = \frac{\langle P_s \rangle}{\langle P_{IP}^e \rangle}, \quad (s = 1-4)$$

(6.7)

(b) For incident SV wave

The energy ratios of the reflected waves (P and SV):

$$E_{RP} = \frac{\langle P_{RP}^e \rangle}{\langle P_{IS}^e \rangle}, \quad E_{RS} = \frac{\langle P_{RS}^e \rangle}{\langle P_{IS}^e \rangle},$$

(6.8)

and the transmitted waves (qP, qSV, qT and eP):

$$ES_s = \frac{\langle P_s \rangle}{\langle P_{IS}^e \rangle}, \quad (s = 1-4)$$

(6.9)

The interaction energy ratios:

for incident P wave: $E_{st} = \dfrac{\langle P_{st} \rangle}{\langle P_{IP}^e \rangle}$, and for incident SV wave: $E_{st} = \dfrac{\langle P_{st} \rangle}{\langle P_{IS}^e \rangle}$

where

$$\langle P_{st} \rangle = \frac{1}{2}\omega^2 \, \mathrm{Re}\left(\Delta_{2s} H_s \bar{H}_t + \Delta_{1s} \bar{W}_t H_s \bar{H}_t + \bar{\Delta}_{6S} \Phi_t H_t \bar{H}_s + \frac{\iota}{\omega} \frac{K_3}{T_0} \bar{\Delta}_{5s} \Theta_s \bar{H}_s H_t \right).$$

(6.10)

The energy is conserved if

$$\sum_{s=1}^{4} \left(ES_s + E_{int} + E_{RP} + E_{RS} \right) = 1$$

(6.11)

where $E_{int} = \displaystyle\sum_{s,t=1, s\neq t}^{4} E_{st}$ is the resultant interaction energy between the refracted waves.

7. Special cases

Case-1: In the context of a perfect normal boundary when $K_t \to \infty$ and $K_n \neq 0$, the modified Δ_{mn} for energy ratios of normal stiffness are presented in Appendix *B*.

Case-2: In the context of a perfect transversal boundary when $K_t \neq 0$ and $K_n \to \infty$, the modified Δ_{mn} for energy ratios of transverse stiffness are presented in Appendix *B*.

Case-3: In the context of a perfect boundary when $K_t \to \infty$ and $K_n \to \infty$, the modified Δ_{mn} for energy ratios of perfect bonding are presented in Appendix *B*.

8. Discussion and numerical findings

Using MATLAB software, the distribution of energy ratios that is brought about by the oncoming of plane waves of the *P* or *SV* types at various angles is calculated by considering a system with an *ES* medium, a material that resembles graphite, and a PVID medium that is close to a material that resembles cadmium selenide to illustrate this technique graphically. For numerical computations, the stiffness parameters are considered as $K_n = 20\,N/m^3$, $K_t = 10\,N/m^3$, and the phase lags are regarded as $\tau_q = 0.06\,s$, $\tau_T = 0.04\,s$ such that they meet the criteria set out by Quintanilla and Racke [36]. Following Kumar and Sharma [37], cadmium selenide and graphite materials material parameters are shown in Tab.1. Viscoelastic constants are given by $\bar{c}_{ij} = c_{ij}\left(1 - \iota F_{ij}\right)$, where $F_{11} = 0.8$, $F_{12} = 0.1$, $F_{13} = 0.6$, $F_{33} = 0.4$, $F_{44} = 0.2$ $\left(Nm^{-2}\right)$.

Table 1. The values of the materials constant.

Symbol	Value	Symbol	Value
K_1	$9\,Wm^{-1}k^{-1}$	K_3	$9\,Wm^{-1}k^{-1}$
β_1	$6.21 \times 10^5\,Nm^{-2}K^{-1}$	β_3	$5.51 \times 10^5\,Nm^{-2}K^{-1}$
β^e	$0.001 \times 10^3\,ms^{-1}$	η_{31}	$-0.160\,Cm^{-2}$
ω	$100\,Hz$	η_{15}	$-0.138\,Cm^{-2}$
ε_{11}	$8.26 \times 10^{-11}\,C^2N^{-1}m^{-2}$	η_{33}	$0.347\,Cm^{-2}$
ε_{33}	$9.03 \times 10^{-11}\,C^2N^{-1}m^{-2}$	C_e	$260\,Jkg^{-1}K^{-1}$
τ_3	$-2.9 \times 10^{-6}\,Cm^{-2}K^{-1}$	c_{11}	$74.1 \times 10^9\,Nm^{-2}$
T_0	$298\,K$	c_{12}	$45.2 \times 10^9\,Nm^{-2}$
α^e	$0.0011 \times 10^3\,ms^{-1}$	c_{13}	$39.3 \times 10^9\,Nm^{-2}$
ρ^e	$2.65 \times 10^3\,kgm^{-3}$	c_{33}	$83.6 \times 10^9\,Nm^{-2}$
ρ	$5504\,kgm^{-3}$	c_{44}	$13.2 \times 10^9\,Nm^{-2}$

The energy distributions of the incident wave (*P*, or *SV*) among different refracted, reflected waves as well as interaction waves for welded contact (WC-DPL), normal stiffness (NS-DPL), transverse stiffness (TS-DPL), and imperfect (II-DPL) interface, in the absence of viscosity are depicted in Figs. (2-25) by dotted red, green, blue, and magenta color lines, respectively. The solid line and the addition of the symbol *V* in the stiffness boundary contacts indicate the existence of viscosity. With the help of MATLAB software, all of these figures have been magnified. E_{RP}, and E_{RS} denoted the energy ratios associated with reflected primary

P, and secondary *SV* waves, respectively, and the transmitted *qP*, *qT*, *qS*, and *eP* waves indicated by ES_i; $i = 1 - 4$, respectively. The E_{int} denoted the ratio of interaction energy among all refracted waves.

8.1. For incident primary *P* wave

Figure 2 reveals that the magnitude of E_{RP} for the imperfect interface follows the sinusoidal path, and the welded contact interface follows the open upward parabolic path corresponding to an angle of incidence $0^0 < \theta_0 \le 90^0$. In contrast, the magnitude of E_{RP} for the TS-DPL and NS-DPL models is close to unity in the whole range of considered angle of incidence θ_0. It is noticed that the magnitude of E_{RP} is high near the normal and grazing incidences in all types of interfaces.
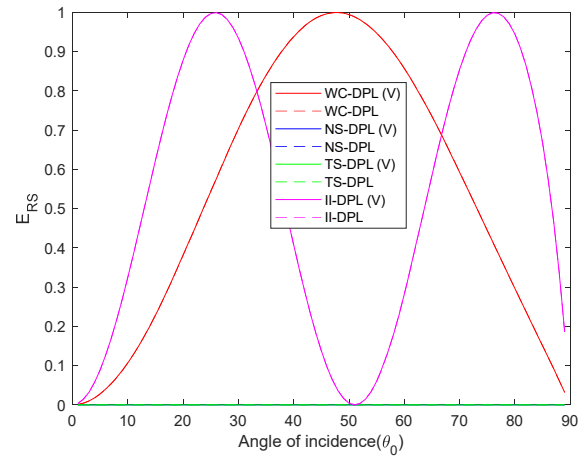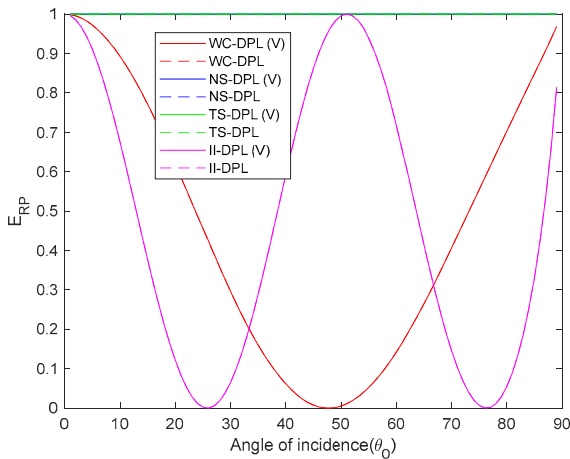
Fig.2. The variability of the energy ratio E_{RP} vs θ_0.   Fig.3. The variability of the energy ratio E_{RS} vs θ_0.

Figure 3 reveals that the magnitude of E_{RS} follows an almost reverse trend as followed by E_{RP} in all considered models. The solid and dotted curves of all four colors are overlaps that indicate that there is no remarkable impact of viscosity.

Figures 4 and 5 demonstrate how the magnitude of ES_1 and ES_2, respectively, increases gradually with the angle of incidence in the presence of viscosity. For all other interfaces other than the welded contact interface, the *qP* and *qS* modes are excited to close to the grazing incidence. As opposed to this, when viscosity is absent, the *qP* and *qS* modes remain in elastic half-space close to normal and grazing incidence, but in the middle range of incidence, the *qP* and *qS* modes become highly significant and move into a piezo-thermoelastic medium. In both cases, when viscosity is present or absent, the *qP* and *qS* modes propagate more readily at the transverse stiffness interface in piezo-thermoelastic media than at other interfaces.

Figures 6 and 7 illustrate that variation in magnitude of ES_3 and ES_4 versus an angle of incidence, respectively. When the viscosity is present, piezo-thermoelastic media with normal and transverse interfaces facilitate rapid propagation of *qT* and *eP* waves in the vicinity of grazing incidence. In the absence of viscosity, *qT* and *eP* modes propagate in a piezo-thermoelastic medium in the mid-range of the angle of incidence for all considered interfaces. In contrast, except for the transverse interface for all other interfaces, *qT* and *eP* modes are intensely stimulated close to the normal incidence, whether viscosity is present or not.

Figure 8 shows that, except for the TS-DPL and II-DPL modes, all models under consideration have an interaction energy ratio maximum near the normal and grazing incidences. In contrast, the maximum interaction energy in these two models occurs at a mid-range of incidence angles.
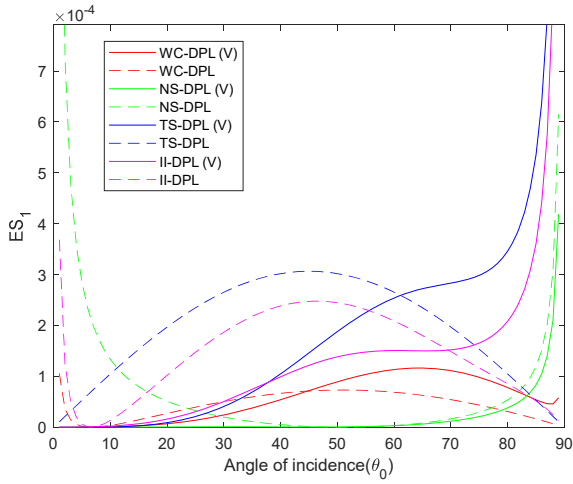
Fig.4. The variability of the energy ratio ES_1 vs θ_0 .
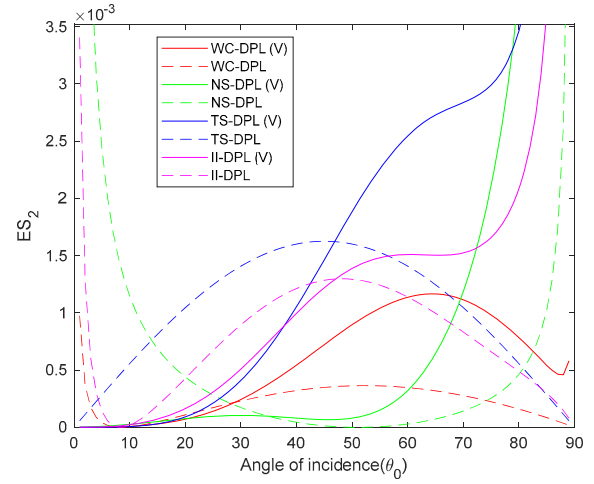
Fig.5. The variability of the energy ratio ES_2 vs θ_0 .
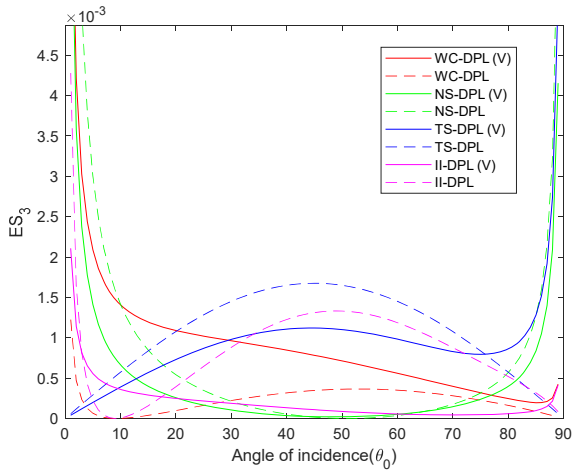
Fig.6. The variability of the energy ratio ES_3 vs θ_0 .
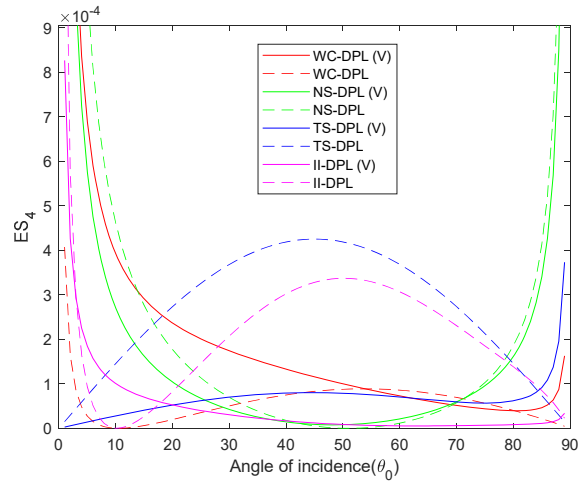
Fig.7. The variability of the energy ratio ES_4 vs θ_0 .
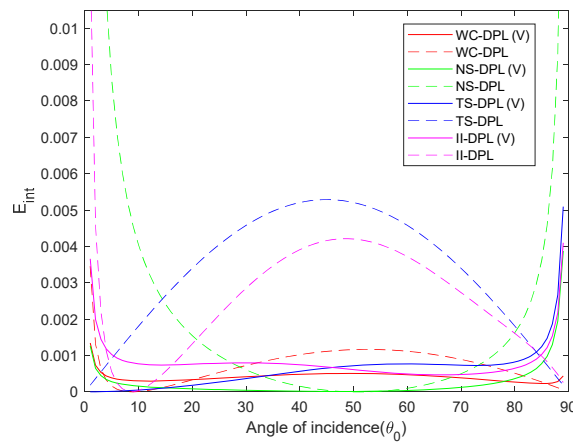
Fig.8. The variability of the energy ratio E_{int} vs θ_0 .

8.2 For incident secondary *SV* wave

Figure 9 shows that the magnitude of E_{RP} for the imperfect interface follows a sinusoidal path, and the welded contact interface follows an open downward parabolic path concerned with the angle of incidence $0 \le \theta_0 \le 66$, $\theta_0 = 66^0$ is the critical angle after the critical angle. In all considered models, the magnitude of the reflected *P* wave is close to zero. In contrast, the magnitude of E_{RP} for the TS-DPL and NS-DPL models is close to zero in the whole range of considered angles of incidence θ_0. Figure 10 reveals that the magnitude of E_{RS} follows an almost reverse trend as followed by E_{RP} in all considered models. The overlaps between the solid and dotted curves in all four colors show that viscosity has no noticeable effect.
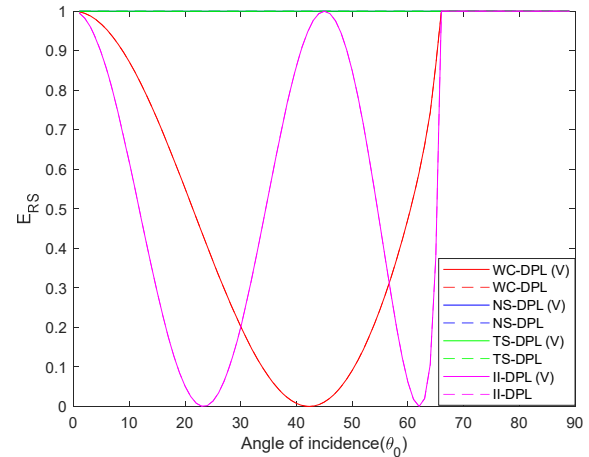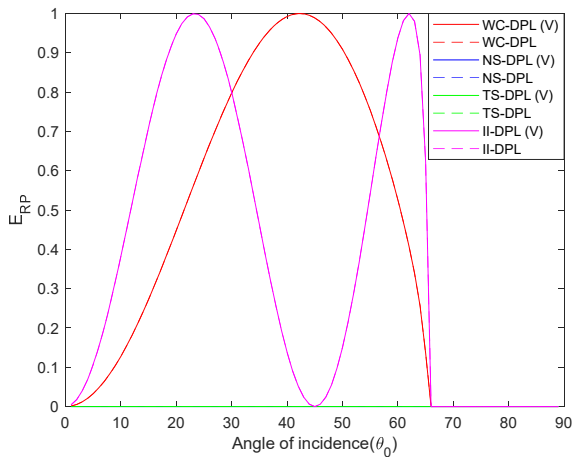
Fig.9. The variability of the energy ratio E_{RP} vs θ_0.

Fig.10. The variability of the energy ratio E_{RS} vs θ_0.
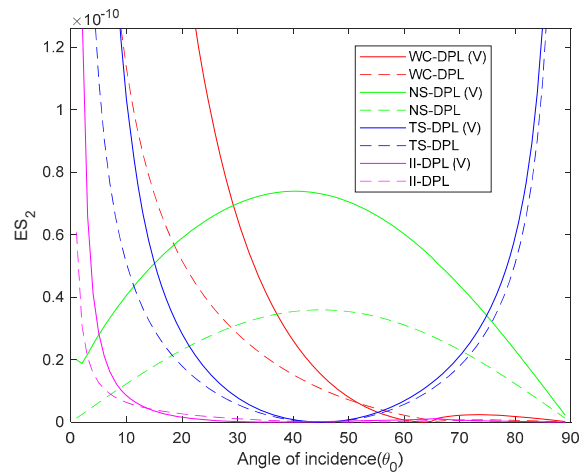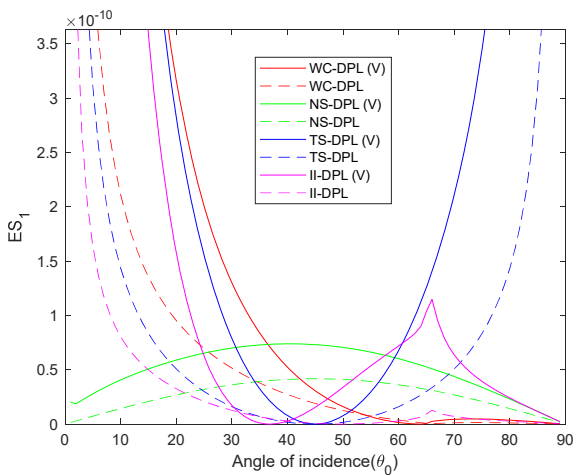
Fig.11. The variability of the energy ratio ES_1 vs θ_0.

Fig.12. The variability of the energy ratio ES_2 vs θ_0.

Figures 11-15 shows how transmission wave energy ratios and interaction wave energy ratios behave in relation to the angle of incidence. All five graphs exhibit a remarkably similar pattern; however, their magnitudes vary depending on the boundaries that are taken into consideration. Except for the normal stiffness interface, for all other interfaces, transmission modes (*qP*, *qS*, *qT*, *eP*) are highly stimulated near the normal incidence and propagate in a piezo-thermoelastic medium. In contrast, near the grazing incidence, except for the transverse stiffness interface, all other interface's transmission modes deactivate and remain in the elastic

half-space. The transmission modes and interaction energy for the transversal interface follow an the upward parabolic route, and the normal interface follows a downward parabolic path. The magnitude of *qP* and *qS* modes in the presence of viscosity is higher than the corresponding interfaces in the absence of viscosity. On the other hand, *qT*, *eP* modes, and interaction energy ratios in the absence of viscosity are more than the corresponding interfaces with the presence of viscosity. A critical angle $\theta_0 = 66^0$ has been observed for the imperfect and welded contact interfaces in both cases, presence or absence of viscosity.
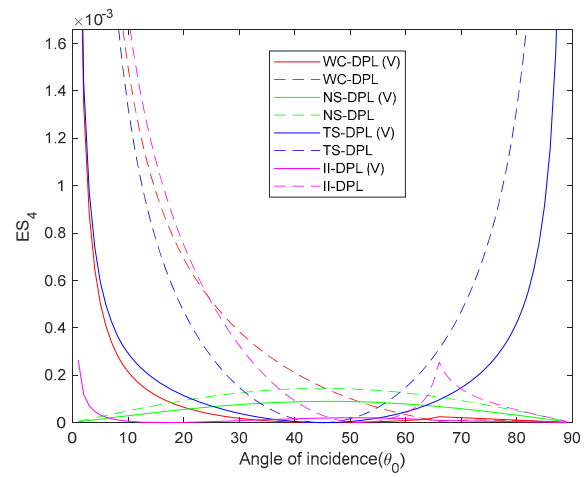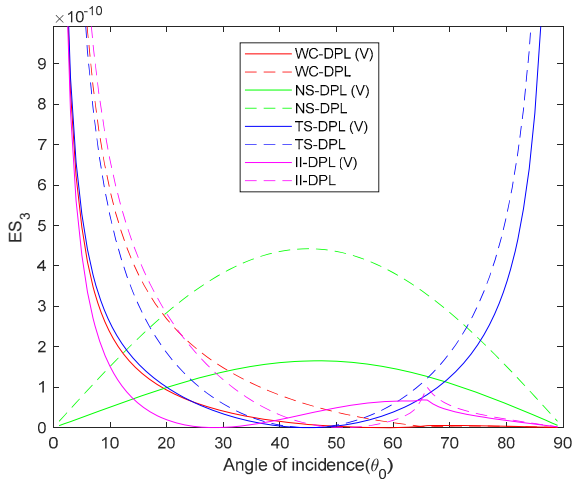
Fig.13. The variability of the energy ratio ES_3 vs θ_0 .   Fig.14. The variability of the energy ratio ES_4 vs θ_0 .
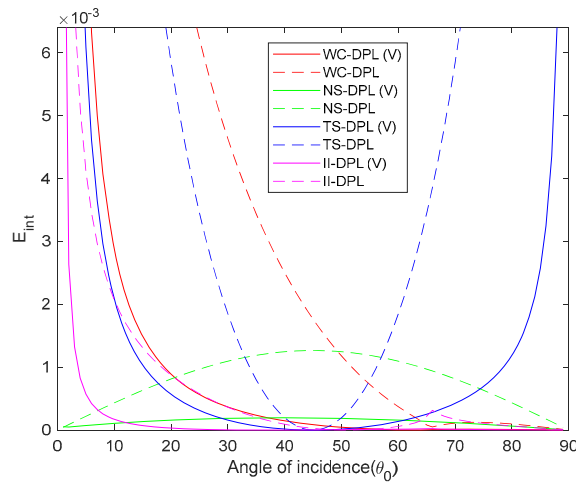
Fig.15. The variability of the energy ratio E_{int} vs θ_0 .

9. Conclusion

This work employs dual-phase lag theory to investigate the propagation of plane waves at an interface of *ES* and PVID. For incident primary *P* or secondary *SV* waves, using the normal mode analysis technique, the energy ratios are computed. Eight different models are created to look into how viscosity and boundary contacts affect energy ratios. Some of the conclusions drawn from this analysis are listed below.

The nature of the incidence wave, viscosity, angle of incidence, and physical characteristics of the material all affect the energy ratios. Figures 2-15 illustrate how the form of this dependency differs for different waves.

The energy ratios E_{RP} and E_{RS} for incidence primary or secondary waves exhibit an almost complete reversal in the entire spectrum of incidence angles. The variability of the magnitudes of E_{RP} and E_{RS} has been observed to be impacted by the different types of assumed interfacial boundaries. However, it has been noted that viscosity has a negligible impact on this phenomenon.

No critical angle for any considered model has been observed for the incidence *P* wave. In contrast, for incidence *SV* wave, there is a critical angle at $\theta = 66^0$ for welded contact, and imperfect interfaces have been observed.

Both cases, for incidence, primary or secondary waves ES_1, ES_2, ES_3, ES_4 and E_{int} follow almost similar trends, but their magnitudes are distinct. The significance of viscosity in determining the energy ratios of interaction and transmitted waves has been established.

Transmitted modes *qP*, *qS*, and *qT* are highly stimulated and easily propagated in the piezo-visco-thermoelastic medium at the transverse stiffness interface compared to other interfaces near the grazing incidence.

The sum of the energy ratios for all eight considered models is close to unity at the whole range of angle of incidence. As a consequence, the law of energy balance is supported by each model.

Nomenclature

C_E	– specific heat at constant strain
c	– apparent phase velocity
c_{ijro}	– elastic stiffness tensor
c_{ijro}^v	– viscoelastic constants
D_i	– electric displacement
E_i	– electric field density
e_{ij}	– component of strain
K_{ij}	– components of thermal conductivity
q	– slowness parameter
T	– thermal temperature
T_0	– reference temperature
u_i	– displacement components
α_{ij}	– coupling constants
β_{ij}	– thermal moduli tensors
$\eta_{ijr}, \varepsilon_{ij}$	– piezothermal moduli tensors
λ, μ	– Lame's constant
ρ	– density
σ_{ij}	– components of the stress tensor
τ_i	– pyroelectric constants
τ_q	– phase lag of heat flux
τ_T	– phase lag of the temperature gradient
φ	– electrical potential

A superscript "*e*" denotes elastic half-space parameters.

Appendix *A*

$$G_{11} = l_{12}l_{22}l_{34}l_{42} + l_{12}l_{23}l_{34}l_{41} ,$$

$$G_{12} = cl_{14}l_{22}l_{34} - cl_{13}l_{23}l_{34} - cl_{13}l_{34}l_{42} - cl_{14}l_{34}l_{41} + a_{41}l_{12}l_{23}l_{34} + a_{24}l_{12}l_{34}l_{41} + a_{43}l_{12}l_{22}l_{34} + l_{11}l_{22}l_{34}l_{42} +$$
$$+ l_{11}l_{23}l_{34}l_{41} + l_{12}l_{21}l_{34}l_{42} - l_{12}l_{22}l_{32}l_{43} + l_{12}l_{22}l_{33}l_{42} - l_{12}l_{23}l_{31}l_{43} + l_{12}l_{23}l_{33}l_{41} + l_{12}l_{24}l_{31}l_{42} - l_{12}l_{24}l_{32}l_{41},$$

$$G_{13} = a_{24}a_{41}l_{12}l_{34} - ca_{41}l_{14}l_{34} - ca_{43}l_{13}l_{34} - ca_{24}l_{13}l_{34} - cl_{13}l_{23}l_{33} + cl_{13}l_{24}l_{32} + cl_{14}l_{21}l_{34} + cl_{14}l_{22}l_{33} + cl_{14}l_{24}l_{31} +$$
$$- cl_{15}l_{22}l_{32} - cl_{15}l_{23}l_{31} + cl_{13}l_{23}l_{43} - cl_{13}l_{24}l_{42} - cl_{14}l_{22}l_{43} - cl_{14}l_{24}l_{41} + cl_{15}l_{22}l_{42} + cm_{15}l_{23} + l_{41} + cl_{13}l_{32}l_{43} +$$
$$- cl_{13}l_{33}l_{42} + cl_{14}l_{31}l_{43} - cl_{14}l_{33}l_{41} + - cl_{15}l_{31}l_{42} + cl_{15}l_{32}l_{41} + a_{41}l_{11}l_{23}l_{34} + a_{41}l_{12}l_{23}l_{33} - a_{41}l_{12}l_{24}l_{32} +$$
$$+ d_{24}l_{11}l_{34}l_{41} - a_{24}l_{12}l_{31}l_{43} + a_{24}l_{12}l_{33}l_{41} + a_{43}l_{11}l_{22}l_{34} + a_{43}l_{12}l_{21}l_{34} + a_{43}l_{12}l_{22}l_{33} + a_{43}l_{12}l_{24}l_{31} + l_{11}l_{21}l_{34}l_{42} +$$
$$- l_{11}l_{22}l_{32}l_{43} + l_{11}l_{22}l_{33}l_{42} - l_{11}l_{23}l_{31}l_{43} + l_{11}l_{23}l_{33}l_{41} + l_{11}l_{24}l_{31}l_{42} - l_{11}l_{24}l_{32}l_{41} - l_{12}l_{21}l_{32}l_{43} + l_{12}l_{21}l_{33}l_{42},$$

$$G_{14} = ca_{41}l_{15}l_{23} - ca_{24}l_{15}l_{31} - ca_{41}l_{14}l_{24} - ca_{24}l_{13}l_{33} + ca_{24}l_{13}l_{43} + ca_{24}l_{15}l_{41} - ca_{43}l_{13}l_{24} + ca_{43}l_{15}l_{22} - ca_{41}l_{14}l_{33} +$$
$$+ ca_{41}l_{15}l_{32} - ca_{43}l_{13}l_{33} - ca_{43}l_{15}l_{31} + a_{24}a_{41}l_{11}l_{34} + a_{24}a_{41}l_{12}l_{33} + cl_{14}l_{21}l_{33} - cl_{15}l_{21} + l_{32} - cl_{14}l_{21}l_{43} +$$
$$+ cl_{15}l_{21}l_{42} + a_{41}l_{11}l_{23}l_{33} - a_{41}l_{11}l_{24}l_{32} - a_{24}l_{11}l_{31}l_{43} + a_{24}l_{11}l_{33}l_{43} + a_{24}l_{11}l_{33}l_{41} + a_{43}l_{11}l_{21}l_{34} + a_{43}l_{11}l_{22}l_{33} +$$
$$+ a_{43}l_{11}l_{24}l_{31} + a_{43}l_{12}l_{21}l_{33} - l_{11}l_{21}l_{32}l_{43} + l_{11}l_{21}l_{33}l_{42},$$

$$G_{15} = ca_{43}l_{15}l_{21} + a_{24}l_{41}l_{11}l_{33} + a_{43}l_{11}l_{21}l_{33} + ca_{24}l_{41}l_{15}.$$

Appendix *B*

Case-1: $\Delta_{3i} = 1$ where $i = 1 - 4$

    (i) For incident *P* wave

$$\Delta_{35} = \frac{\iota\omega\sin\theta_0}{\alpha^*}, \qquad \Delta_{36} = \frac{\iota\omega\cos\theta_2}{\beta^*}.$$

    (ii) For incident *SV* wave

$$\Delta_{35} = \frac{\iota\omega\sin\theta_1}{\alpha^*}, \qquad \Delta_{36} = \frac{\iota\omega\cos\theta_0}{\beta^*}.$$

Case-2: $\Delta_{4i} = W_i$ where $i = 1 - 4$

    (i) For incident *P* wave

$$\Delta_{45} = -\frac{\iota\omega\cos\theta_0}{\alpha^*}, \qquad \Delta_{46} = \frac{\iota\omega\sin\theta_2}{\beta^*}.$$

    (ii) For incident *SV* wave

$$\Delta_{45} = -\frac{\iota\omega\cos\theta_1}{\alpha^*}, \qquad \Delta_{46} = \frac{\iota\omega\sin\theta_0}{\beta^*}.$$

Case-3: $\Delta_{3i} = 1$, $\Delta_{4i} = W_i$ where $i = 1 - 4$

    (i) For incident *P* wave

$$\Delta_{35} = \frac{\iota\omega\sin\theta_0}{\alpha^*}, \qquad \Delta_{36} = \frac{\iota\omega\cos\theta_2}{\beta^*}, \qquad \Delta_{45} = -\frac{\iota\omega\cos\theta_0}{\alpha^*}, \qquad \Delta_{46} = \frac{\iota\omega\sin\theta_2}{\beta^*}.$$

    (ii) For incident *SV* wave

$$\Delta_{35} = \frac{\iota\omega\sin\theta_I}{\alpha^*}, \qquad \Delta_{36} = \frac{\iota\omega\cos\theta_0}{\beta^*}, \qquad \Delta_{45} = -\frac{\iota\omega\cos\theta_I}{\alpha^*}, \qquad \Delta_{46} = \frac{\iota\omega\sin\theta_0}{\beta^*}.$$

Acknowledgment

References

[1] Mindlin R.D. (1974): *Equations of high frequency vibrations of thermopiezoelectric crystal plates.*– Int. J. Solids Struct., vol.10, No.6, pp.625-637.

[2] Nowacki W. (1978): *Some general theorems of thermopiezoelectricity.*– J. Therm. Stress., vol.1, No. 2, pp.171-182.

[3] Nowacki W. (1979): *Foundation of Linear Piezoelectricity.*– In: H. Parkus, editor. *Electro-magnetic interactions in elastic solids.* Chapter 1. Springer, Wein.

[4] Chandrasekharaiah D.S. (1988): *A generalized linear thermoelasticity theory for piezoelectric media.*– Acta Mech., vol.71, No.1-4, pp.39-49.

[5] Pang Y., Wang Y.S., Liu J.X. and Fang D.N. (2008): *Reflection and refraction of plane waves at the interface between piezoelectric and piezomagnetic media.*– Int. J. Eng. Sci., vol.46, No.11, pp.1098-1110.

[6] Kuang Z.B. and Yuan X.G. (2011): *Reflection and transmission of waves in pyroelectric and piezoelectric materials.*– J. Sound Vib., vol.330, No.6, pp.1111-1120.

[7] Abd-alla A. El Nour N., Hamdan A.M., Giorgio I. and Del Vescovo D. (2014): *The mathematical model of reflection and refraction of longitudinal waves in thermo-piezoelectric materials.*– Arch. Appl. Mech., vol.84, No.9-11, pp.1229-1248.

[8] Yadav A.K., Barak, M.S., and Gupta V. (2023): *Reflection at the free surface of the orthotropic piezo-hygro-thermo-elastic medium.*– International Journal of Numerical Methods for Heat & Fluid Flow, vol.33, No.10, pp.3535-3560.

[9] Gupta V. and Barak M.S. (2023): *Photo-thermo-piezo-elastic waves in semiconductor medium subject to distinct two temperature models with higher order memory dependencies.*– International Journal of Numerical Methods for Heat & Fluid Flow, vol.34, No.4, DOI:10.1108/HFF-07-2023-0380.

[10] Pathania V., Kumar R., Gupta V. and Barak M.S. (2022): *Generalized Plane Waves in a Rotating Thermoelastic Double Porous Solid*, Int. J. Appl. Mech. Eng., vol.27, No.4, pp.138-154.

[11] Pathania V., Kumar R., Gupta V., and Barak M.S. (2023): *Double porous thermoelastic waves in a homogeneous, isotropic solid with inviscid liquid.*– Arch. Appl. Mech., vol.93, pp.1943-1962.

[12] Gupta V., Kumar R., Kumar M., Pathania V. and Barak M.S. (2023): *Reflection/transmission of plane waves at the interface of an ideal fluid and nonlocal piezothermoelastic medium.*– Int. J. Numer. Methods Heat Fluid Flow, vol.33, No.2, pp.912-937.

[13] Barak M.S., Kumar R., Kumar R. and Gupta V. (2023): *The effect of memory and stiffness on energy ratios at the interface of distinct media.*– Multidiscip. Model. Mater. Struct., vol.19, No.3, pp.464-492.

[14] Gupta V., Kumar R., Kumar R. and Barak M.S. (2023): *Energy analysis at the interface of piezo/thermoelastic half spaces.*– Int. J. Numer. Methods Heat Fluid Flow, vol.33, No.6, pp.2250-2277.

[15] Barak M.S., Kumar R., Kumar R. and Gupta V. (2023): *Energy analysis at the boundary interface of elastic and piezothermoelastic half-spaces.*– Indian J. Phys., vol.97, pp.2369-2383.

[16] Barak M.S. and Gupta V. (2023): *Memory-dependent and fractional order analysis of the initially stressed piezo-thermoelastic medium.*– Mech. Adv. Mater. Struct., pp.1-15, https://doi.org/10.1080/15376494.2023.2211065.

[17] Gupta V. and Barak M.S. (2023): *Quasi-P wave through orthotropic piezo-thermoelastic materials subject to higher order fractional and memory-dependent derivatives.*– Mech. Adv. Mater. Struct., pp.1-15, https://doi.org/10.1080/15376494.2023.2217420.

[18] Voigt W. (1887): *Theoretical Studies on the Elasticity of Crystals.*– Royal Society of Sciences in Göttingen.

[19] Gurtin E., Morton E. and Sternberg E. (1962): *On the Linear Theory of Viscoelasticity.*– Brown Univ. Provid. Ri. Div. Appl. Math.

[20] Atabek H.B. and Lew H.S. (1966): *Wave propagation through a viscous incompressible fluid contained in an initially stressed elastic tube.*– Biophys. J., vol.6, No.4, pp.481-503.

[21] Sharma K.D., Kumar R., Kakkar M.K. and Ghangas S. (2021): *Three dimensional waves propagation in thermo-viscoelastic medium with two temperature and void.*– IOP Conf. Ser. Mater. Sci. Eng., vol.1033, No.1, p.012059.

[22] Abouelregal A.E., Ahmad H., Yao S.W. and Abu-Zinadah H. (2021): *Thermo-viscoelastic orthotropic constraint cylindrical cavity with variable thermal properties heated by laser pulse via the MGT thermoelasticity model.*– Open Phys., vol.19, No.1, pp.504-518.

[23] Abouelregal A.E., Ahmad H., Badr S.K., Almutairi B. and Almohsen B. (2022): *Viscoelastic stressed microbeam analysis based on Moore-Gibson-Thompson heat equation and laser excitation resting on Winkler foundation.*– J. Low Freq. Noise Vib. Act. Control, vol.41, No.1, pp.118-139.

[24] Mirsky I. (1967): *Wave propagation in a viscous fluid contained in an orthotropic elastic tube.*– Biophys. J., vol.7, No.2, pp.165-186.

[25] Atabek H.B. (1968): *Wave propagation through a viscous fluid contained in a tethered, initially stressed, orthotropic elastic tube.*– Biophys. J., vol.8, No.5, pp.626-649.

[26] Yasein M., Mabrouk N., Lotfy K. and El-Bary A.A. (2019): *The influence of variable thermal conductivity of semiconductor elastic medium during photothermal excitation subjected to thermal ramp type.*– Results Phys., vol.15, pp.102766.

[27] Lotfy K., El-Bary A.A. and Tantawi R.S. (2019): *Effects of variable thermal conductivity of a small semiconductor cavity through the fractional order heat-magneto-photothermal theory.*– Eur. Phys. J. Plus, vol.134, No.6, pp.280.

[28] Lotfy K. and Tantawi R.S. (2020): *Photo-thermal-elastic interaction in a functionally graded material (FGM) and magnetic field.*– Silicon, vol.12, No.2, pp.295-303.

[29] Lotfy K., Elidy E.S. and Tantawi R.S. (2021): *Piezo-photo-thermoelasticity transport process for hyperbolic two-temperature theory of semiconductor material.*– Int. J. Mod. Phys. C, vol.32, No.07, pp. 2150088.

[30] Mahdy A.M.S., Lotfy K., El-Bary A. and Tayel I.M. (2021): *Variable thermal conductivity and hyperbolic two-temperature theory during magneto-photothermal theory of semiconductor induced by laser pulses.*– Eur. Phys. J. Plus, vol.136, No.6, pp.651.

[31] Mahdy A.M.S., Gepreel K.A., Lotfy K. and El-Bary A.A. (2021): *A numerical method for solving the Rubella ailment disease model.*– Int. J. Mod. Phys. C, vol.32, No.7, pp.2150097.

[32] Tzou D.Y. (1995): *A unified field approach for heat conduction from macro- to micro-scales.*– J. Heat Transfer, vol.117, pp.8-16.

[33] Achenbach J.D. (1973): *Wave Propagation in Elastic Solids.*– Amsterdam: North Holland.

[34] Biot M.A. (1956): *Thermoelasticity and irreversible thermodynamics.*– J. Appl. Phys., vol.27, No.3, pp.240-253.

[35] Lord H.W. and Shulman Y. (1967): *A generalized dynamical theory of thermoelasticity.*– J. Mech. Phys. Solids, vol.15, No.5, pp.299-309.

[36] Quintanilla R. and Racke R. (2006): *Qualitative aspects in dual-phase-lag thermoelasticity.*– SIAM J. Appl. Math., vol.66, No.3, pp.977-1001.

[37] Kumar R. and Sharma P. (2021): *Response of two-temperature on the energy ratios at elastic-piezothermoelastic interface.*– J. Solid Mech., vol.13, No.2, pp.186-201.